

Manipulating the orbital-angular-momentum correlation of entangled two-photon states in three-dimensional nonlinear photonic crystals

Chuan Xu ¹, Songtao Huang ¹, Qian Yu ¹, Dunzhao Wei ², Pengcheng Chen,¹ Saiwei Nie ¹,
Yong Zhang ^{1,*} and Min Xiao ^{1,3}

¹*National Laboratory of Solid State Microstructures, College of Engineering and Applied Sciences, School of Physics, and Collaborative Innovation Center of Advanced Microstructures, Nanjing University, Nanjing 210093, China*

²*School of Physics, Sun Yat-sen University, Guangzhou 510275, China*

³*Department of Physics, University of Arkansas, Fayetteville, Arkansas 72701, USA*



(Received 30 July 2021; accepted 9 December 2021; published 27 December 2021)

Three-dimensional (3D) nonlinear photonic crystal (NPC) has recently been realized in experiment, which provides a powerful platform for quantum-state engineering. Here, we propose a fork-grating 3D NPC scheme to manipulate orbital-angular-momentum (OAM) correlations of entangled two-photon pairs. The spiral spectra, bandwidths, and generation rates of counterpropagating and copropagating photon pairs are theoretically analyzed. Our results show that 3D NPC is of practical significance to generate high-dimensional OAM entanglement for quantum precision measurement, quantum computing, and quantum communication.

DOI: [10.1103/PhysRevA.104.063716](https://doi.org/10.1103/PhysRevA.104.063716)

I. INTRODUCTION

Spontaneous parametric down-conversion (SPDC) in nonlinear crystals is a common method to obtain entangled two-photon pairs, which plays a key role in fundamental quantum physics, quantum information, quantum metrology, and quantum imaging [1–6]. In SPDC, a strong pump light produces two lower-frequency photons (referred to as signal and idler), which obeys the conservation law of energy and momentum. The entanglement of the two-photon state has been realized in polarizations [7], time bins [8], paths [9], and transverse spatial modes [10]. The dimension of the path entanglement has been increased to 100 recently [11].

One convenient and direct way for high-dimensional entanglement is based on the orbital-angular-momentum (OAM) correlation between signal and idler photons in SPDC. The spatial modes carrying OAM of $l\hbar$ (here, l is any integer value) suitably encode high-dimensional quantum information [12] by utilizing the discrete nature of OAM in infinite-dimensional Hilbert space. High-dimensional OAM entanglement has been applied for quantum precision measurement [13–15], quantum spiral imaging [16,17], tests of the 12-dimensional generalized Bell inequalities [18], as well as providing resilience to noise [19]. In experiment, it is generally to produce high-dimensional OAM correlation by shaping the pump light [20–22].

Quasi-phase-matching (QPM) engineering was proposed for the spatial manipulation of entangled two-photon states in two-dimensional (2D) nonlinear photonic crystals (NPCs) [23]. Such crystals provide a compact and stable platform for quantum-state engineering [24–28], such as the generations of high-dimensional path-entangled states [26,28] and

narrow-band counterpropagating entangled photons [29], and the on-chip manipulation of entangled two-photon states [25]. However, limited by traditional fabrication techniques, 2D NPCs can only provide reciprocal-lattice vectors (RLVs) in two dimensions. Because the manipulation of two-photon OAM states needs 2D RLVs for full wave-front modulation, the QPM condition generally cannot be maintained in this case. Therefore, the output of two-photon OAM states from 2D NPC usually has low efficiency, limiting the brightness of the source [13]. Recently, three-dimensional (3D) NPCs produced using a femtosecond laser engineering technique provide a potential solution to an efficient spatial modulation in 3D QPM configuration for the generation of high-dimensional entanglement [30–35].

In this paper, we theoretically investigate the manipulation of the spiral spectrum of entangled photon pairs within a fork-grating 3D NPC. In comparison to 2D NPC case, the spectral bandwidth of the entangled photon pairs can be greatly decreased in a 3D NPC. The conversion efficiency is also significantly enhanced by several orders of magnitude. In addition, we propose the schemes to generate high-dimensional maximally entangled OAM states within 3D NPCs. Our results show that 3D NPC is capable of producing and spatially steering two-photon pairs simultaneously and efficiently, thereby paving the way to integrate high-dimensional entangled quantum light source in quantum-state engineering.

II. DESCRIPTION OF THE SPDC PROCESS IN A FORK-GRATING 3D NPC

We consider a type-0 ($e e e$) SPDC process. The 3D NPC of fork grating can be fabricated by using femtosecond-laser erasing technique [36,37] in a z -cut lithium niobate (LiNbO₃)

*zhangyong@nju.edu.cn

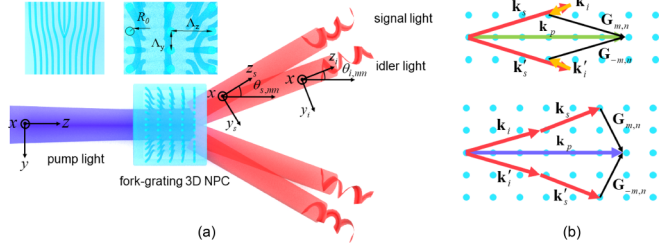


FIG. 1. (a) Schematic of the SPDC process in a fork-grating 3D NPC. (b) The QPM configurations for counterpropagating (top) and copropagating (bottom) entangled photon pairs.

crystal [Fig. 1(a)]. The second-order nonlinear coefficient function $\chi^2(\mathbf{r})$ in 3D NPC is [38]

$$\chi^2(\mathbf{r}) = \eta d_{33} \sum_{m,n} F_{m,n} \exp(-imG_y y - inG_z z) \exp(iml_c \varphi), \quad (1)$$

with

$$F_{m,n} = \frac{R_0}{\sqrt{(m\Lambda_z)^2 + (n\Lambda_y)^2}} J_1 \left(R_0 \sqrt{(mG_y)^2 + (nG_z)^2} \right), \quad (2)$$

where η denotes the erasing efficiency of femtosecond-laser writing, d_{33} the nonlinear coefficient of the LiNbO₃ crystal, $F_{m,n}$ the Fourier coefficients of the RLV $\mathbf{G}_{m,n} = mG_y \hat{\mathbf{y}} + nG_z \hat{\mathbf{z}}$ ($m, n = 0, \pm 1, \pm 2, \dots$) with $G_y = 2\pi/\Lambda_y$, and $G_z = 2\pi/\Lambda_z$, l_c the topological charge (TC) of the fork-grating structure in NPC, $\varphi = \tan^{-1}(y/x)$ the azimuthal angle in the x - y plane, $J_1(\xi)$ the first-order Bessel function, Λ_y (Λ_z) the structure period along the y (z) direction, and R_0 the radius of the erased domain [Fig. 1(a)].

The interaction Hamiltonian \hat{H}_I of SPDC is written as

$$\hat{H}_I = \varepsilon_0 \int_V d^3\mathbf{r} \chi^2(\mathbf{r}) E_p^{(+)} E_s^{(-)} E_i^{(-)} + \text{H.c.}, \quad (3)$$

where ε_0 denotes the vacuum permittivity, $E^{(+)}$ and $E^{(-)}$ denote the positive- and negative-frequency parts of the electric field, respectively, H.c. means the Hermitian conjugate of the previous term, the subscripts p, s, i on the electric field intensities refer, respectively, to the pump, signal, and idler beams, and V denotes the interaction volume. Treating the pump light as a classical field of a single frequency, the formulas for the electric fields are

$$E_p^{(+)} = E_p \exp(ik_{pz}z - i\omega_p t) f(x, y), \quad (4)$$

$$E_j^{(-)} = \sum_{\mathbf{k}_j} E_j \exp(-i\mathbf{k}_j \cdot \mathbf{r} + i\omega_j t) \hat{a}_j^\dagger(\mathbf{k}_j), \quad (j = s, i), \quad (5)$$

with

$$E_j = \sqrt{\hbar\omega_j/2\varepsilon_0 V n_j^2}, \quad (6)$$

where \hat{a}^\dagger , ω , n , and \mathbf{k} denote the creation operator, angular frequency, crystal refractive index, and wave vector of the

electric field, respectively, $f(x, y)$ and E_p denote the transverse profile function and the amplitude of the pump light, and $k_{pz} = K_p - |\kappa_p|^2/2K_p$ denotes the longitudinal wave number inside the crystal, with κ_p being the transverse wave vector of the pump field and $K_p = n_p\omega_p/c$. The conservation law of energy holds, $\omega_p = \omega_s + \omega_i$, where $\omega_s = \Omega_s + \nu_s$. Ω_s and ν_s denote the central frequency and deviation of the signal beam, respectively. The wave vector of the signal beam is

$$\mathbf{k}_s = \mathbf{k}_{szs} + \boldsymbol{\kappa}_s, \quad (7)$$

with

$$\mathbf{k}_{szs} = k_{szs} (-\sin\theta_{s,mn} \hat{\mathbf{y}} + \cos\theta_{s,mn} \hat{\mathbf{z}}), \quad (8)$$

$$k_{szs} = K_s + \frac{\nu_s}{u_s} - \frac{|\boldsymbol{\kappa}_s|^2}{2K_s}, \quad (9)$$

$$\boldsymbol{\kappa}_s = \kappa_{sx} \hat{\mathbf{x}} + \kappa_{sy_s} \cos\theta_{s,mn} \hat{\mathbf{y}} + \kappa_{sy_s} \sin\theta_{s,mn} \hat{\mathbf{z}}, \quad (10)$$

where $|\mathbf{k}_{szs}^0| \gg |\boldsymbol{\kappa}_s|$, and $K_s = n_s\Omega_s/c$, $\theta_{s,mn}$ denotes the angle between the central wave vectors \mathbf{k}_{szs} and the z axis in the y - z plane, $\boldsymbol{\kappa}_s$ the transverse wave vector of the signal beam in the x - y_s plane, u_s the group velocity of signal beam, the subscript mn is in reference to $\mathbf{G}_{m,n}$, and $\kappa_{sx}(\kappa_{sy_s})$ denotes the component of the signal-field transverse wave vector along the x (y_s) direction. Similar expressions hold for the idler beam.

We assume that the area of the crystal illuminated by the pump light is sufficiently large. From the first-order perturbation theory, we have an entangled two-photon state:

$$\begin{aligned} |\psi\rangle &= AL \sum_{m,n} F_{m,n} \int d\omega_s \int d\omega_i \delta(\omega_s + \omega_i - \omega_p) \\ &\times \iint d^2\boldsymbol{\kappa}_s \iint d^2\boldsymbol{\kappa}_i F(\Delta k_{tr,x}, \Delta k_{tr,y}) \\ &\times \exp(i\Delta k_z L/2) \text{sinc}(\Delta k_z L/2) \hat{a}^\dagger(\boldsymbol{\kappa}_s) \hat{a}^\dagger(\boldsymbol{\kappa}_i) |0\rangle, \end{aligned} \quad (11)$$

with

$$\begin{aligned} F(\Delta k_{tr,x}, \Delta k_{tr,y}) &= \iint dx dy f(x, y) \exp(iml_c \varphi) \\ &\times \exp[-i(\Delta k_{tr,x} x + \Delta k_{tr,y} y)], \end{aligned} \quad (12)$$

where the coefficient $A \propto \eta d_{33}$, L denotes the crystal length,

$$\Delta k_{tr,x} = \kappa_{sx} + \kappa_{ix}, \quad (13)$$

$$\begin{aligned} \Delta k_{tr,y} &= -\Delta k_{tr,y}^0 - \frac{\nu_s}{u_s} \sin\theta_{s,mn} \\ &- \frac{\nu_i}{u_i} \sin\theta_{i,mn} + \kappa_{sy_s} \cos\theta_{s,mn} \\ &+ \kappa_{iy_i} \cos\theta_{i,mn} + \frac{\kappa_s^2}{2K_s} \sin\theta_{s,mn} + \frac{\kappa_i^2}{2K_i} \sin\theta_{i,mn}, \end{aligned} \quad (14)$$

$$\begin{aligned} \Delta k_z &= \Delta k_z^0 - \frac{\nu_s}{u_s} \cos\theta_{s,mn} - \frac{\nu_i}{u_i} \cos\theta_{i,mn} \\ &- \kappa_{sy_s} \sin\theta_{s,mn} - \kappa_{iy_i} \sin\theta_{i,mn} \\ &- \frac{\kappa_p^2}{2K_p} + \frac{\kappa_s^2}{2K_s} \cos\theta_{s,mn} + \frac{\kappa_i^2}{2K_i} \cos\theta_{i,mn}, \end{aligned} \quad (15)$$

$$\Delta k_{tr,y}^0 = K_s \sin \theta_{s,mn} + K_i \sin \theta_{i,mn} - mG_y, \quad (16)$$

$$\Delta k_z^0 = K_p - K_s \cos \theta_{s,mn} - K_i \cos \theta_{i,mn} - nG_z, \quad (17)$$

and under the 3D QPM condition, $\Delta k_{tr,y}^0 = \Delta k_z^0 = 0$.

Next, we analyze the bandwidth of the entangled photons in a fork-grating 3D NPC. We consider a structure that satisfies the QPM conditions for the generation of counterpropagating entangled photons. As shown in Fig. 1(b), the counterpropagating signal and idler beams are collinear, i.e., $\theta_{s,mn} = \pi - \theta_{i,mn} = \theta_{mn}$, and the angle θ_{mn} is small enough (i.e., $\cos \theta_{mn} = 1$). In this type-0 (*e e e*) SPDC, we consider nondegenerate frequencies of signal and idler beams, i.e., $\Omega_s \neq \Omega_i$, and $\nu_s = -\nu_i = \nu$ because of the conservation law of energy. Then, the parameters of the two-photon state in Eq. (11) become

$$\Delta k_{tr,x} = \kappa_{sx} + \kappa_{ix}, \quad (18)$$

$$\Delta k_{tr,y} = \kappa_{sy} - \kappa_{iy}, \quad (19)$$

$$\Delta k_z = -D\nu + \bar{\nu}, \quad (20)$$

with

$$D = \frac{1}{u_s} + \frac{1}{u_i}, \quad (21)$$

$$\bar{\nu} = -\frac{\kappa_p^2}{2K_p} + \frac{\kappa_s^2}{2K_s} + \frac{\kappa_i^2}{2K_i}. \quad (22)$$

The joint spectral density for the two-photon state is

$$h(\Delta k_z L) = \left| \text{sinc} \left(\frac{(-D\nu + \bar{\nu})L}{2} \right) \right|^2, \quad (23)$$

and the corresponding bandwidth is $\Delta\omega = 1.77\pi/DL$.

Under such counterpropagation configuration, one can obtain narrow-band nondegenerate two-photon state. Here, we set $\lambda_p = 532$ nm, $\lambda_s = 795$ nm, and $\lambda_i = 1550$ nm for example. The 795-nm signal photon is compatible to atomic system for quantum storage and the 1550-nm photon can be used for long-distance fiber quantum communication. We use a fork-grating 3D NPC with $\Lambda_y = 8\mu\text{m}$, $\Lambda_z = 0.35\mu\text{m}$, and $R_0 = 0.134\mu\text{m}$ for calculations. The involved RLV is $\mathbf{G}_{\pm 1,1}$ for QPM. The working temperature of 3D NPC is 81.9°C . By using a 2-cm-long 3D NPC, the spectral bandwidth of the counterpropagating photons is calculated to be $\Delta\omega = 2\pi \times 3.06$ GHz, which is greatly reduced in comparison to

the 2D NPC case [13,39–41]. In addition, we also numerically simulate the copropagating entangled photons ($\theta_{s,mn} = \theta_{i,mn} = \theta_{mn}$). The fork-grating 3D NPC has $\Lambda_y = 8\mu\text{m}$, $\Lambda_z = 12\mu\text{m}$, $R_0 = 2.548\mu\text{m}$. The crystal temperature is 104.6°C . The calculated bandwidth is $\Delta\omega = 2\pi \times 347$ GHz.

III. MANIPULATION OF THE OAM CORRELATION IN A FORK-GRATING 3D NPC

In a SPDC process, the signal and idler photons are OAM correlated, forming a spiral spectrum of the two-photon states. One can manipulate the OAM correlation in a fork-grating 3D NPC. We consider two QPM configurations, i.e., the entangled photons are counterpropagating ($\theta_{s,mn} = \pi - \theta_{i,mn} = \theta_{mn}$) and copropagating ($\theta_{s,mn} = \theta_{i,mn} = \theta_{mn}$) (Fig. 1). For simplicity, the signal and idler beams are assumed to be monochromatic, which can be justified by using narrow-band filters in front of the detectors [42]. With a small angle θ_{mn} , the SPDC processes satisfy the OAM conservation laws, i.e., $l_p + ml_c = l_s \pm l_i$, where \pm corresponds to forward (backward propagation) of the idler photon [39,43]. Because the OAM-carrying Laguerre-Gaussian (LG) mode set is complete and orthogonal, we decompose a two-photon state $|\psi\rangle$ at the pump beam waist ($z = 0$) in the LG basis [44],

$$|\psi\rangle = \sum_{l_s, p_s} \sum_{l_i, p_i} C_{p_s, p_i}^{l_s, l_i} |l_s, p_s; l_i, p_i\rangle, \quad (24)$$

with

$$C_{p_s, p_i}^{l_s, l_i} = \langle l_s, p_s; l_i, p_i | \psi \rangle, \quad (25)$$

where $|l_s, p_s; l_i, p_i\rangle = \iint d^2\kappa_s \iint d^2\kappa_i \widetilde{\text{LG}}_{p_s}^{l_s}(\kappa_s) \widetilde{\text{LG}}_{p_i}^{l_i}(\kappa_i) \times \hat{a}^\dagger(\kappa_s) \hat{a}^\dagger(\kappa_i) |0\rangle$, $\widetilde{\text{LG}}_p^l(\kappa)$ denotes the Fourier transform of the LG function $\text{LG}_p^l(\rho)$, and $C_{p_s, p_i}^{l_s, l_i}$ the probability amplitude to detect the signal photon in the mode of $\widetilde{\text{LG}}_{p_s}^{l_s}(\kappa_s)$ and the idler photon in the mode of $\widetilde{\text{LG}}_{p_i}^{l_i}(\kappa_i)$. Considering that $|C_{p_s, p_i}^{l_s, l_i}|^2$ corresponds to the weight in the LG basis, one can calculate the normalized spiral spectrum. We assume that the Rayleigh range of the pump light is much larger than the 3D NPC length L , i.e., under the thin crystal approximation [45,46], and the pump light is in an $\text{LG}_{p_p}^{l_p}(\rho)$ mode. With a certain RLV $\mathbf{G}_{m,n}$ satisfying the QPM conditions of Eqs. (16) and (17) with a small θ_{mn} , we obtain (see the Appendix)

$$\begin{aligned} C_{p_s, p_i}^{l_s, l_i} &\propto LF_{m,n} \sqrt{\frac{8p_p! p_s! p_i! (|l_p| + p_p)! (|l_s| + p_s)! (|l_i| + p_i)!}{\pi}} \delta_{l_p + ml_c, l_s \pm l_i} \frac{1}{w_p^3} \left(\frac{\sqrt{2}}{w_p} \right)^{|l_p| + |l_s| + |l_i|} \\ &\times \gamma_s^{|l_s| + 1} \gamma_i^{|l_i| + 1} \sum_{j_p=0}^{p_p} \sum_{j_s=0}^{p_s} \sum_{j_i=0}^{p_i} \left(-\frac{2}{w_p^2} \right)^{j_p + j_s + j_i} \frac{1}{(|l_p| + j_p)! j_p! (p_p - j_p)!} \\ &\times \frac{\gamma_s^{2j_s} \gamma_i^{2j_i}}{(|l_s| + j_s)! j_s! (p_s - j_s)! (|l_i| + j_i)! j_i! (p_i - j_i)!} P(\sigma, \beta), \end{aligned} \quad (26)$$

with

$$P(\sigma, \beta) = \int_0^\infty d\rho \exp(-\beta\rho^2)\rho^\sigma = \begin{cases} \frac{\sqrt{\pi}}{2^\sigma} \frac{\sigma!}{(\sigma/2)!} \left(\frac{1}{\beta}\right)^{(\sigma+1)/2}, & \sigma \text{ is even,} \\ \left(\frac{\sigma-1}{2}\right)! \left(\frac{1}{\beta}\right)^{(\sigma+1)/2}, & \sigma \text{ is odd,} \end{cases} \quad (27)$$

where j_p , j_s , and j_i are positive integers, $\sigma = |l_p| + |l_s| + |l_i| + 2(j_p + j_s + j_i) + 1$, $\beta = (1 + \gamma_s^2 + \gamma_i^2)/w_p^2$, $\gamma_s = w_p/w_s$, and $\gamma_i = w_p/w_i$, with w_p , w_s , and w_i being the waists of the pump, signal, and idler beams, respectively. In Eq. (26), the Kronecker delta function $\delta_{l_p+ml_c, l_s \pm l_i}$ ensures the OAM conservation law, i.e., $l_p + ml_c = l_s \pm l_i$. For counterpropagating (copropagating) photons, the OAM correlation between signal and idler photons is positive (negative). Notably, the TC of NPC structure (l_c) takes part in the OAM conservation, which distinguishes this work from the method of shaping the pump light [47]. Figure 2 compares the spiral spectra by shaping the pump light ($l_c = 0$, $l_p \neq 0$) and introducing fork-grating 3D NPC structure ($l_p = 0$, $l_c \neq 0$). Here, the pump beam is in an $LG_0^{l_p}(\rho)$ mode and the involved RLV is $\mathbf{G}_{1,1}$. We use $p_s = p_i = 0$ and $\gamma_s = \gamma_i = 1$ in detection. The spiral bandwidth by shaping the pump light in Figs. 2(a) and 2(b) is wider than that modulated by 3D NPC in Figs. 2(c) and 2(d). This can be attributed to the intensity profile of the pump light.

Figure 3 shows the spiral spectra with $\mathbf{G}_{-1,1}$ and $\mathbf{G}_{1,1}$. Here, $p_s = p_i = 0$, $\gamma_s = \gamma_i = 1$, $l_c = 2$, and $l_p = 1$. With different RLVs, the OAM correlation between signal and idler photons stays positive (negative) for counterpropagation

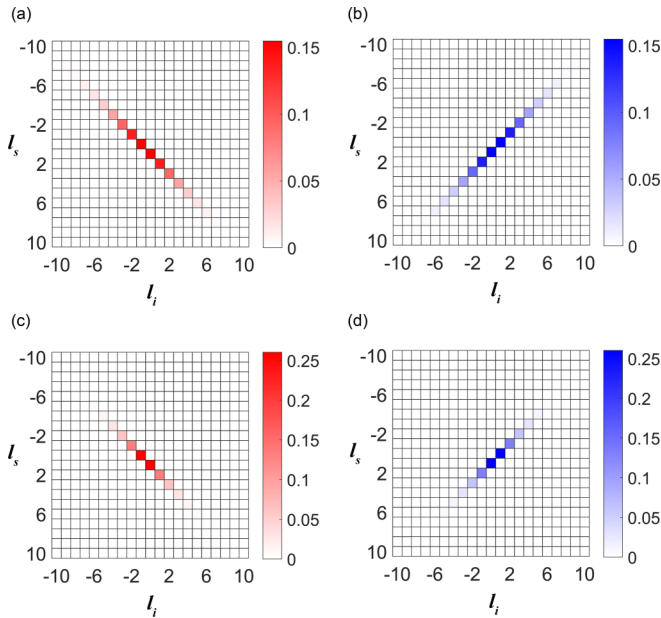


FIG. 2. Normalized spiral spectra for counterpropagation (red, left side) and copropagation (blue, right side) QPM configurations with $p_s = p_i = 0$ and $\gamma_s = \gamma_i = 1$ in detection. (a) and (b) correspond to the method of shaping the pump light ($l_c = 0$, $l_p = 1$), in which the phase matching condition is satisfied by using a 1D NPC. (c) and (d) correspond to the method of using forkgrating 3D NPC ($l_c = 1$, $l_p = 0$). The color bars show the weights in the LG basis.

(copropagation) situation. The spiral spectra of $\mathbf{G}_{-1,1}$ and $\mathbf{G}_{1,1}$ are different in the spiral spectral profiles and the central values of l_s and l_i . This results from different OAM conservation conditions, i.e., $l_p - l_c = l_s \pm l_i$ for $\mathbf{G}_{-1,1}$ and $l_p + l_c = l_s \pm l_i$ for $\mathbf{G}_{1,1}$.

Next, we analyze the probability amplitude of two-photon pair. In 2D NPC (Fig. 4), two reasons limit the source brightness. First, the QPM condition is not fully satisfied ($\Delta k_z^0 \neq 0$) and the effective length is limited to $\pi/\Delta k_z^0$. Second, the interacting waves do not couple via the maximum nonlinear coefficient d_{33} . In comparison, it is feasible to achieve $\Delta k_z^0 = 0$ and utilize d_{33} in a 3D NPC. In addition, one can increase the 3D NPC length to enhance brightness because the conversion efficiency is proportional to the square of the crystal length in 3D NPC.

We design a 3D NPC for copropagating configuration according to the reported femtosecond laser erasing technique [32]. The 3D NPC structure [Fig. 1(a)] is fabricated inside a z -cut 5% MgO-doped LiNbO₃ crystal. The carried TC is $l_c = 1$. The laser erasing efficiency is $\eta = 0.15$ [32]. In the y - z plane, the structure period is $\Lambda_z = \Lambda_y = 3 \mu\text{m}$ and the radius of the erased domain is $R_0 = 0.81 \mu\text{m}$ [Fig. 1(a)]. The RLVs $\mathbf{G}_{-1,1}$ and $\mathbf{G}_{1,1}$ take part in a type-0 ($e e e$) SPDC process. The corresponding Fourier coefficient is $F_{\pm 1,1} = 0.0993$. The NPC temperature is stabilized at 37.9 °C. The pump wavelength is 417.3 nm. The generation rate with $\mathbf{G}_{1,1}$ of 3D NPC is

$$R \propto |\eta d_{33} L F_{1,1}|^2. \quad (28)$$

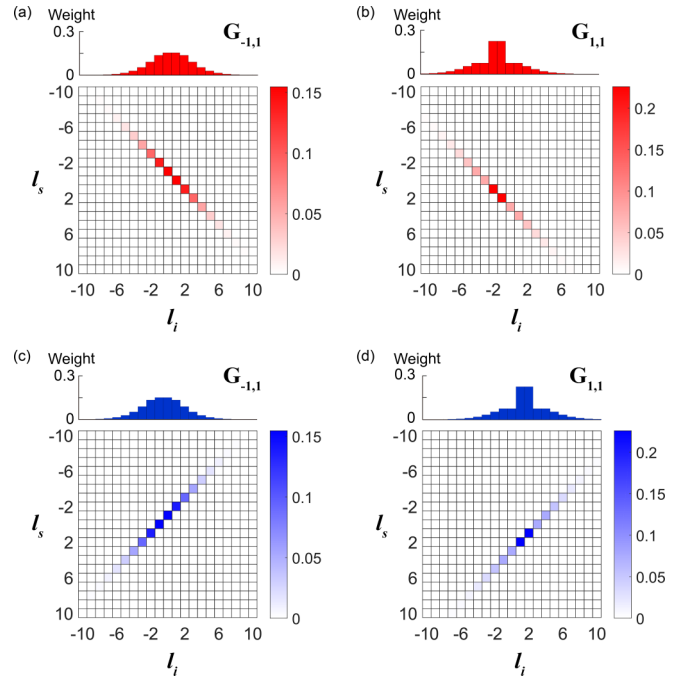


FIG. 3. Normalized spiral spectra with $\mathbf{G}_{-1,1}$ and $\mathbf{G}_{1,1}$ to satisfy the QPM condition under (a), (b) counterpropagation (red, top side) and (c), (d) copropagation (blue, bottom side). Here, $p_s = p_i = 0$, $\gamma_s = \gamma_i = 1$, $l_c = 2$ and $l_p = 1$. The insets show the spiral spectral profiles of the idler photons. The color bars show the weights in the LG basis.

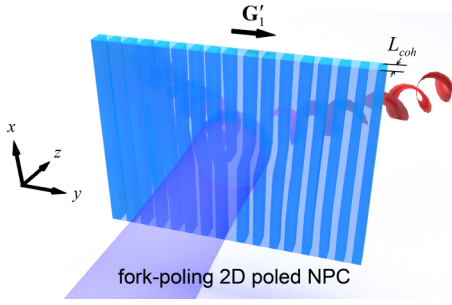


FIG. 4. Fork-grating 2D poled NPC with a length of $L_{\text{coh}} = \pi/\Delta k_z = 1.5 \mu\text{m}$ and a period of $\Lambda_y = 3 \mu\text{m}$. The duty cycle is 1/2 and the Fourier coefficient \mathbf{G}'_1 is $F'_1 = 0.3185$.

We use a fork-grating 2D poled NPC (Fig. 4) for comparison. The first-order RLV \mathbf{G}'_1 in the transvers direction is utilized. The generation rate is $R' \propto |2d_{22}L_{\text{coh}}F'_1|^2$. The ratio of the generation rates in 3D NPC and 2D NPC is

$$\frac{R}{R'} \propto \left| \frac{\eta d_{33} L F_{1,1}}{2d_{22} L_{\text{coh}} F'_1} \right|^2, \quad (29)$$

where $d_{33} = 27.2 \text{ pm/V}$ and $d_{22} = 2.1 \text{ pm/V}$ in LiNbO_3 crystal [48]. Using a $200\text{-}\mu\text{m}$ -long 3D LiNbO_3 NPC, the generation rate of the two-photon state is enhanced by three orders of magnitude compared with that in 2D NPC. Consider that a 100-mW pump light is focused into a spot of 0.01 mm^2 and is then injected into this 3D NPC. The coincidence rate for the generated photons is calculated to be 175 s^{-1} with 1-nm narrow-band filters in front of the detectors. Notably, the experimental realization requires to increase the length of 3D NPC to enhance the conversion efficiency.

IV. THREE-DIMENSIONAL NPC SCHEME FOR GENERATING HIGH-DIMENSIONAL MAXIMALLY ENTANGLED OAM STATES

High-dimensional maximally entangled OAM states are common sources for quantum key distribution [49] and quantum communication [50,51]. Because of the nonuniformity of the spiral bandwidth, researchers usually postselect high-dimensional maximally entangled OAM states via entanglement concentration applying Procrustean methods, which, however, reduces the detection efficiency [18,51,52]. Recently, shaping the pump light to obtain a three-dimensional maximally entangled state (MES) has been demonstrated [20,21]. However, it requires strict optimization in shaping the pump light, i.e., constructing its superposition modes, which makes it difficult for practical applications. With 3D NPC, one can directly and efficiently generate MESs with a single-mode pump light. Here, we give two examples with $p_s = p_i = 0$ and $\gamma_s = \gamma_i = 1$ in detection. First, for the situation of counterpropagation two-photon, we use an LG-mode pump light with $l_p = -1$ and $p_p = 0$ to pass through a fork-grating 3D NPC with $l_c = 1$. The RLV $\mathbf{G}_{1,1}$ is involved in the SPDC process, which can generate a three-dimensional maximally entangled OAM state, i.e., $|\psi\rangle = (|-1, -1\rangle + |0, 0\rangle + |1, 1\rangle)/\sqrt{3}$.

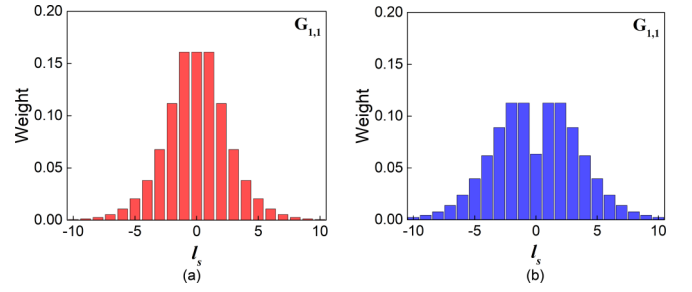


FIG. 5. Normalized spiral spectra of an entangled two-photon state for counterpropagation (red, left side) and copropagation (blue, right side) QPM configurations with $p_s = p_i = 0$ and $\gamma_s = \gamma_i = 1$ in detection. (a) $l_c = -l_p = 1$, and (b) $l_c = -l_p = 2$.

Here, the numbers in the ket vector refer to OAM quanta. The spiral spectrum is shown in Fig. 5(a). Second, a copropagating four-dimensional maximally entangled OAM state, i.e., $|\psi\rangle = (|-2, 2\rangle + |-1, 1\rangle + |1, -1\rangle + |2, -2\rangle)/2$, can be produced when $l_c = -l_p = 2$ and $p_p = 0$ [Fig. 5(b)]. Our simulation shows that 3D NPC is a promising platform to generate high-dimensional maximally entangled OAM states.

V. CONCLUSION

We have theoretically analyzed the spiral spectra of the counterpropagating and copropagating entangled two-photon states generated from a fork-grating 3D NPC. In comparison to previous works, the proposed method is efficient and has unique spiral spectral characteristics. Our simulations also demonstrate that 3D NPC is a potential platform to generate narrow-band high-dimensional maximally entangled OAM states. Furthermore, with properly designed structures of 3D NPC, such as spiral structure and cascade structure [53], one can utilize wavelength, polarization, time bin, and path for multidimensional entanglement, which yields high information capacity in quantum key distribution and quantum communication [49–51,54]. Three-dimensional NPC is a competitive candidate for quantum-state engineering.

ACKNOWLEDGMENTS

This work was supported by the National Key R&D Program of China (Grants No. 2021YFA1400803 and No. 2017YFA0303703), the National Natural Science Foundation of China (NSFC) (Grants No. 91950206, No. 11874213, and No. 11904424), and Fundamental Research Funds for the Central Universities (Grants No. 021314380191 and No. 021314380105). We thank Prof. Y. Cai and Dr. J. Tang for useful discussions.

APPENDIX: LAGUERRE-GAUSSIAN MODE DECOMPOSITION OF ENTANGLED PHOTON STATES

Consider that an $\text{LG}_{p_p}^{l_p}(\rho)$ -mode pump light illuminates the 3D NPC, the RLV $\mathbf{G}_{m,n}$ is used to complete QPM condition, and $\cos\theta_{mn} = 1$. Substituting Eqs. (11)–(17) into Eq. (25),

we obtain in radial coordinates the coefficient $C_{p_s, p_i}^{l_s, l_i}$ at the beam waist ($z = 0$),

$$\begin{aligned} C_{p_s, p_i}^{l_s, l_i} &= AL \sum_{m, n} F_{m, n} \int d\omega_s \int d\omega_i \delta(\omega_s + \omega_i - \omega_p) \\ &\times \iint d^2\kappa'_s \iint d^2\kappa'_i \iint d^2\kappa_s \iint d^2\kappa_i F(\Delta k_{tr, x}, \Delta k_{tr, y}) \widetilde{LG}_{p_s}^{l_s*}(\kappa'_s) \widetilde{LG}_{p_i}^{l_i*}(\kappa'_i) \\ &\times \exp\left(i \frac{\Delta k_z L}{2}\right) \text{sinc}\left(\frac{\Delta k_z L}{2}\right) \delta(\kappa'_s - \kappa_s) \delta(\kappa'_i - \kappa_i), \end{aligned} \quad (\text{A1})$$

with

$$F(\Delta k_{tr, x}, \Delta k_{tr, y}) = \iint dx dy LG_p^l(x, y) \exp(iml_c \varphi) \exp[-i(\Delta k_{tr, x} x + \Delta k_{tr, y} y)], \quad (\text{A2})$$

$$\Delta k_{tr, x} = \kappa_{sx} + \kappa_{ix}, \quad (\text{A3})$$

$$\Delta k_{tr, y} = \kappa_{sy} \pm \kappa_{iy}, \quad (\text{A4})$$

where \pm corresponds to forward (backward) propagation of the idler photon,

$$LG_p^l(\rho) = \sqrt{\frac{2p!}{\pi(|l| + p)!}} \frac{1}{w} \left(\frac{\sqrt{2}\rho}{w}\right)^{|l|} L_p^{|l|}\left(\frac{2\rho^2}{w^2}\right) \exp\left(-\frac{\rho^2}{w^2}\right) \exp(il\varphi). \quad (\text{A5})$$

Here, $\widetilde{LG}_p^l(\kappa)$ denotes the Fourier transform of $LG_p^l(\rho)$, l and p are the azimuthal and radial indices, respectively. w is the waist of the LG mode beam, and $L_p^{|l|}(x)$ is the associated Laguerre polynomial [47]. We denote the waists of the pump, signal, and idler beams by w_p , w_s , and w_i . Under the thin crystal approximation, we can ignore the *sinc* function in Eq. (A1). In the spatial domain, the coefficient $C_{p_s, p_i}^{l_s, l_i}$ is expressed as

$$C_{p_s, p_i}^{l_s, l_i} \propto LF_{m, n} \int_0^{2\pi} d\varphi \int_0^\infty \rho d\rho LG_{p_p}^l(\rho, \varphi) LG_{p_s}^{l_s*}(\rho, \varphi) LG_{p_i}^{l_i*}(\rho, \varphi) \exp(iml_c \varphi). \quad (\text{A6})$$

After calculating Eq. (A6), we obtain

$$\begin{aligned} C_{p_s, p_i}^{l_s, l_i} &\propto LF_{m, n} \sqrt{\frac{8p_p! p_s! p_i! (|l_p| + p_p)! (|l_s| + p_s)! (|l_i| + p_i)!}{\pi}} \delta_{l_p + m, l_s \pm l_i} \frac{1}{w_p^3} \left(\frac{\sqrt{2}}{w_p}\right)^{|l_p| + |l_s| + |l_i|} \\ &\times \gamma_s^{|l_s| + 1} \gamma_i^{|l_i| + 1} \sum_{j_p=0}^{p_p} \sum_{j_s=0}^{p_s} \sum_{j_i=0}^{p_i} \left(-\frac{2}{w_p^2}\right)^{j_p + j_s + j_i} \frac{1}{(|l_p| + j_p)! j_p! (p_p - j_p)!} \\ &\times \frac{\gamma_s^{2j_s} \gamma_i^{2j_i}}{(|l_s| + j_s)! j_s! (p_s - j_s)! (|l_i| + j_i)! j_i! (p_i - j_i)!} P(\sigma, \beta), \end{aligned} \quad (\text{A7})$$

where j_p , j_s , and j_i are positive integers, $\gamma_s = w_p/w_s$ and $\gamma_i = w_p/w_i$ are the ratios of the pump beam waist to the respective signal and idler beam waists, and

$$P(\sigma, \beta) = \int_0^\infty d\rho \exp(-\beta\rho^2) \rho^\sigma = \begin{cases} \frac{\sqrt{\pi}}{2^\sigma} \frac{\sigma!}{(\sigma/2)!} \left(\frac{1}{\beta}\right)^{(\sigma+1)/2}, & \sigma \text{ is even,} \\ \frac{(\sigma-1)!}{2^\sigma} \left(\frac{1}{\beta}\right)^{(\sigma+1)/2}, & \sigma \text{ is odd,} \end{cases} \quad (\text{A8})$$

with $\sigma = |l_p| + |l_s| + |l_i| + 2(j_p + j_s + j_i) + 1$ and $\beta = (1 + \gamma_s^2 + \gamma_i^2)/w_p^2$.

- [1] Z. Y. Ou and L. Mandel, *Phys. Rev. Lett.* **61**, 50 (1988).
 [2] Y. H. Shih and C. O. Alley, *Phys. Rev. Lett.* **61**, 2921 (1988).
 [3] D. Bouwmeester, J.-W. Pan, K. Mattle, M. Eibl, H. Weinfurter, and A. Zeilinger, *Nature (London)* **390**, 575 (1997).
 [4] I. Afek, O. Ambar, and Y. Silberberg, *Science* **328**, 879 (2010).
 [5] T. B. Pittman, Y. H. Shih, D. V. Strekalov, and A. V. Sergienko, *Phys. Rev. A* **52**, R3429 (1995).

- [6] G. B. Lemos, V. Borish, G. D. Cole, S. Ramelow, R. Lapkiewicz, and A. Zeilinger, *Nature (London)* **512**, 409 (2014).
 [7] P. G. Kwiat, K. Mattle, H. Weinfurter, A. Zeilinger, A. V. Sergienko, and Y. Shih, *Phys. Rev. Lett.* **75**, 4337 (1995).
 [8] J. D. Franson, *Phys. Rev. Lett.* **62**, 2205 (1989).
 [9] A. Rossi, G. Vallone, A. Chiuri, F. De Martini, and P. Mataloni, *Phys. Rev. Lett.* **102**, 153902 (2009).

- [10] A. Mair, A. Vaziri, G. Weihs, and A. Zeilinger, *Nature (London)* **412**, 313 (2001).
- [11] L. Li, Z. Liu, X. Ren, S. Wang, V.-C. Su, M.-K. Chen, C. H. Chu, H. Y. Kuo, B. Liu, W. Zang *et al.*, *Science* **368**, 1487 (2020).
- [12] L. Allen, M. W. Beijersbergen, R. J. C. Spreeuw, and J. P. Woerdman, *Phys. Rev. A* **45**, 8185 (1992).
- [13] Y. Ming, J. Tang, Z. Chen, F. Xu, L. Zhang, and Y. Lu, *IEEE J. Sel. Top. Quantum Electron.* **21**, 225 (2015).
- [14] S. Xiao, L. Zhang, D. Wei, F. Liu, Y. Zhang, and M. Xiao, *Opt. Express* **26**, 1997 (2018).
- [15] C. Xu, L. Zhang, S. Huang, T. Ma, F. Liu, H. Yonezawa, Y. Zhang, and M. Xiao, *Photonics Res.* **7**, A14 (2019).
- [16] L. Torner, J. P. Torres, and S. Carrasco, *Opt. Express* **13**, 873 (2005).
- [17] N. Uribe-Patarroyo, A. Fraine, D. S. Simon, O. Minaeva, and A. V. Sergienko, *Phys. Rev. Lett.* **110**, 043601 (2013).
- [18] A. C. Dada, J. Leach, G. S. Buller, M. J. Padgett, and E. Andersson, *Nat. Phys.* **7**, 677 (2011).
- [19] S. Ecker, F. Bouchard, L. Bulla, F. Brandt, O. Kohout, F. Steinlechner, R. Fickler, M. Malik, Y. Guryanova, R. Ursin *et al.*, *Phys. Rev. X* **9**, 041042 (2019).
- [20] E. V. Kovlakov, S. S. Straupe, and S. P. Kulik, *Phys. Rev. A* **98**, 060301(R) (2018).
- [21] S. Liu, Z. Zhou, S. Liu, Y. Li, Y. Li, C. Yang, Z. Xu, Z. Liu, G. Guo, and B. Shi, *Phys. Rev. A* **98**, 062316 (2018).
- [22] Y. Chen, W. Zhang, D. Zhang, X. Qiu, and L. Chen, *Phys. Rev. Appl.* **14**, 054069 (2020).
- [23] J. P. Torres, A. Alexandrescu, S. Carrasco, and L. Torner, *Opt. Lett.* **29**, 376 (2004).
- [24] X. Q. Yu, P. Xu, Z. D. Xie, J. F. Wang, H. Y. Leng, J. S. Zhao, S. N. Zhu, and N. B. Ming, *Phys. Rev. Lett.* **101**, 233601 (2008).
- [25] H. Y. Leng, X. Q. Yu, Y. X. Gong, P. Xu, Z. D. Xie, H. Jin, C. Zhang, and S. N. Zhu, *Nat. Commun.* **2**, 429 (2011).
- [26] H. Jin, P. Xu, X. W. Luo, H. Y. Leng, Y. X. Gong, W. J. Yu, M. L. Zhong, G. Zhao, and S. N. Zhu, *Phys. Rev. Lett.* **111**, 023603 (2013).
- [27] H. Jin, F. M. Liu, P. Xu, J. L. Xia, M. L. Zhong, Y. Yuan, J. W. Zhou, Y. X. Gong, W. Wang, and S. N. Zhu, *Phys. Rev. Lett.* **113**, 103601 (2014).
- [28] E. Megidish, A. Halevy, H. S. Eisenberg, A. Ganany-Padowicz, N. Habshoosh, and A. Arie, *Opt. Express* **21**, 6689 (2013).
- [29] Y.-X. Gong, Z.-D. Xie, P. Xu, X.-Q. Yu, P. Xue, and S.-N. Zhu, *Phys. Rev. A* **84**, 053825 (2011).
- [30] D. Wei, C. Wang, H. Wang, X. Hu, D. Wei, X. Fang, Y. Zhang, D. Wu, Y. Hu, J. Li *et al.*, *Nat. Photonics* **12**, 596 (2018).
- [31] T. Xu, K. Switkowski, X. Chen, S. Liu, K. Koynov, H. Yu, H. Zhang, J. Wang, Y. Sheng, and W. Krolikowski, *Nat. Photonics* **12**, 591 (2018).
- [32] D. Wei, C. Wang, X. Xu, H. Wang, Y. Hu, P. Chen, J. Li, Y. Zhu, C. Xin, X. Hu *et al.*, *Nat. Commun.* **10**, 4193 (2019).
- [33] S. Liu, K. Switkowski, C. Xu, J. Tian, B. Wang, P. Lu, W. Krolikowski, and Y. Sheng, *Nat. Commun.* **10**, 3208 (2019).
- [34] Y. Zhang, Y. Sheng, S. Zhu, M. Xiao, and W. Krolikowski, *Optica* **8**, 372 (2021).
- [35] P. Chen, C. Wang, D. Wei, Y. Hu, X. Xu, J. Li, D. Wu, J. Ma, S. Ji, L. Zhang *et al.*, *Light: Sci. Appl.* **10**, 146 (2021).
- [36] J. Thomas, V. Hilbert, R. Geiss, T. Pertsch, A. Tünnermann, and S. Nolte, *Laser Photon. Rev.* **7**, L17 (2013).
- [37] S. Kroesen, K. Tekce, J. Imbrock, and C. Denz, *Appl. Phys. Lett.* **107**, 101109 (2015).
- [38] A. Arie, N. Habshoosh, and A. Bahabad, *Opt. Quantum Electron.* **39**, 361 (2007).
- [39] L. L. Lu, P. Xu, M. L. Zhong, Y. F. Bai, and S. N. Zhu, *Opt. Express* **23**, 1203 (2015).
- [40] N. V. Bloch, K. Shemer, A. Shapira, R. Shiloh, I. Juwiler, and A. Arie, *Phys. Rev. Lett.* **108**, 233902 (2012).
- [41] S. Trajtenberg-Mills, A. Karnieli, N. Voloch-Bloch, E. Megidish, H. S. Eisenberg, and A. Arie, *Laser Photonics Rev.* **14**, 1900321 (2020).
- [42] J. P. Torres, G. Molina-Terriza, and L. Torner, *J. Opt. B: Quantum Semiclass. Opt.* **7**, 235 (2005).
- [43] J. P. Torres, C. I. Osorio, and L. Torner, *Opt. Lett.* **29**, 1939 (2004).
- [44] J. P. Torres, A. Alexandrescu, and L. Torner, *Phys. Rev. A* **68**, 050301(R) (2003).
- [45] S. Franke-Arnold, S. M. Barnett, M. J. Padgett, and L. Allen, *Phys. Rev. A* **65**, 033823 (2002).
- [46] F. M. Miatto, D. Giovannini, J. Romero, S. Franke-Arnold, S. M. Barnett, and M. J. Padgett, *Eur. Phys. J. D* **66**, 178 (2012).
- [47] A. M. Yao, *New J. Phys.* **13**, 053048 (2011).
- [48] V. G. Dmitriev, G. G. Gurzadyan, and D. N. Nikogosyan, *Handbook of Nonlinear Optical Crystals* (Springer-Verlag, Berlin, 1999), p. 125.
- [49] A. K. Ekert, *Phys. Rev. Lett.* **67**, 661 (1991).
- [50] A. Vaziri, G. Weihs, and A. Zeilinger, *Phys. Rev. Lett.* **89**, 240401 (2002).
- [51] A. Vaziri, J.-W. Pan, T. Jennewein, G. Weihs, and A. Zeilinger, *Phys. Rev. Lett.* **91**, 227902 (2003).
- [52] C. H. Bennett, H. J. Bernstein, S. Popescu, and B. Schumacher, *Phys. Rev. A* **53**, 2046 (1996).
- [53] A. Riazzi, C. Chen, E. Y. Zhu, A. V. Gladyshev, P. G. Kazansky, J. E. Sipe, and L. Qian, *npj Quantum Inf.* **5**, 77 (2019).
- [54] C. Daniele, P. Emanuele, V. Mauro, C. Gonzalo, B. Davide, S. Nicolò, K. K. O. Leif, and S. Fabio, *Adv. Photonics* **1**, 046005 (2019).